Erciyes University Journal of Institue Of Science and Technology

Research Article
10.65520/erciyesfen.1934731

Imprint:
Volume: 42(2)
Year: 2026
Page: 761-786

Ali SAKMAK[a*]
Yavuz CANBAY[b]

[a] Master's Student, Kahramanmaras Sutcu Imam University, alisakmak@gmail.com
[b] Assoc. Prof., Kahramanmaras Sutcu Imam University, yavuzcanbay@ksu.edu.tr

[*] Corresponding Author

Received: 4/20/2026
Accepted: 7/13/2026

Citation:
Ali SAKMAK, Yavuz CANBAY (2026). Synthetic MRI as an Alternative Training Resource for Brain Tumor Classification: A GAN-Based Study. *Erciyes University Journal of Institute Of Science and Technology*, 42(2), 761-786. https://doi.org/10.65520/erciyesfen.1934731

Screened by iThenticate for Authors & Researchers

Synthetic MRI as an Alternative Training Resource for Brain Tumor Classification: A GAN-Based Study

Abstract

Accurate classification of brain tumors from magnetic resonance (MR) imaging data very important for clinical decision support systems. However, the privacy issues encountered in MR data and the high cost of data collection processes make it difficult to develop artificial intelligence-based detection systems. Hence, synthetic data generation has emerged as a promising solution to mitigate data scarcity while preserving patient privacy. This study evaluates the feasibility of using synthetic MRI data as an alternative training resource and compares real, synthetic, and combined data for training scenarios under a unified experimental framework. Moreover, synthetic data generation is considered not only as a mechanism for performance enhancement but also as a potential approach for supporting privacy-sensitive medical imaging applications where access to real patient data may be restricted. In this paper, three experimental scenarios were considered: real MR images only, GAN-generated synthetic MR images only, and a hybrid dataset combining both. Transfer learning models were used and their classification success was evaluated using various metrics. The findings show that models perform better with synthetic images alone, while in some models, using original and synthetic data together can have a positive impact on performance. These results demonstrate that GAN-generated synthetic images can provide meaningful data diversity and may serve as an alternative training resource in medical image classification tasks, particularly in scenarios where access to real data is limited.

Keywords: *Tumor Detection, Transfer Learning, Data Privacy, GAN*

Beyin Tümörü Sınıflandırması için Alternatif Bir Eğitim Kaynağı Olarak Sentetik MRI: GAN Tabanlı Bir Çalışma

Öz

Manyetik rezonans (MR) görüntüleme verilerinden beyin tümörlerinin doğru sınıflandırılması, klinik karar destek sistemleri için büyük önem taşımaktadır. Bununla birlikte, MR verilerinde karşılaşılan mahremiyet sorunları ve veri toplama süreçlerinin yüksek maliyeti, yapay zekâ tabanlı tespit sistemlerinin geliştirilmesini zorlaştırmaktadır. Bu bağlamda, sentetik veri üretimi, hasta mahremiyetini korurken veri kıtlığını hafifletmek için umut vadeden bir çözüm olarak ortaya çıkmıştır. Bu çalışma, alternatif bir eğitim kaynağı olarak sentetik MR verilerinin kullanılabilirliğini değerlendirmekte ve gerçek, sentetik ve birleştirilmiş eğitim senaryolarını birleşik bir deneysel çerçeve altında karşılaştırmaktadır. Ayrıca, sentetik veri üretimi yalnızca bir performans artırma mekanizması olarak değil, aynı zamanda gerçek hasta verilerine erişimin kısıtlanabileceği mahremiyet açısından hassas tıbbi görüntüleme uygulamalarını desteklemek için potansiyel bir yaklaşım olarak da ele alınmaktadır. Bu makalede üç deneysel senaryo ele alınmıştır: yalnızca gerçek MR görüntüleri, yalnızca GAN tarafından üretilen sentetik MR görüntüleri ve her ikisini birleştiren hibrit bir veri kümesi. Transfer öğrenme modelleri eğitilmiş ve sınıflandırma başarıları çeşitli ölçütler kullanılarak değerlendirilmiştir. Bulgular, modellerin yalnızca sentetik görüntülerle daha iyi performans gösterdiğini, bazı modellerde ise orijinal ve sentetik verilerin birlikte kullanılmasının performansı olumlu etkileyebileceğini göstermektedir. Bu sonuçlar, GAN tarafından üretilen sentetik görüntülerin anlamlı veri çeşitliliği sağlayabileceğini ve özellikle gerçek verilere erişimin sınırlı olduğu senaryolarda tıbbi görüntü sınıflandırma görevlerinde alternatif bir eğitim kaynağı olarak kullanılabileceğini göstermektedir.

Anahtar kelimeler: *Tümör tespiti, Transfer Öğrenme, Veri Mahremiyeti, GAN*

1. INTRODUCTION

A tumor is the abnormal growth of cells and tissues [1]. Brain tumors are pathological conditions that directly affect the functioning of the brain, the most complex and sensitive region of the central nervous system, and have a high mortality rate. Early detection of these tumors is important for treatment success. However, the diversity of tumor structures makes early diagnosis quite difficult due to the potential for rapid progression and limited symptoms. Therefore, magnetic resonance imaging is widely used in the diagnosis of brain tumors due to its superior properties in terms of soft tissue contrast. According to the World Health Organization, tumors can spread from one part of the body to another and threaten a person's life [2].

Manual interpretation performed by radiologists in traditional diagnostic processes is time-consuming and may also vary depending on individual expertise differences [3]. Therefore, computer-aided diagnosis systems are being developed to improve, accelerate and standardize diagnostic processes. Especially with the rapid emergence of artificial intelligence in recent years, these systems have become widespread. Architectures such as convolutional neural networks (CNNs) in deep learning have demonstrated significant success in the classification of brain tumors using labeled data sets [4]. Due to their structure, brain tumors are difficult to detect early [5].

However, in the field of Medical Imaging, especially in areas containing personal health data such as brain MRI images, access to sufficiently large data sets has always been a serious problem. Patient privacy, ethical rules, and regulations regarding data sharing limit access to data and the use of models. This limits generalization ability and negatively affects practical use [6]. Consequently, class imbalances observed in data sets cause a bias in the training of models and reveal weaknesses in transferring results obtained in experimental environments to practical settings [7].

In order to solve these problems, various data augmentation techniques are frequently used in the literature. These techniques generally involve rotating, reflecting, and changing attributes such as brightness and contrast of images. But, these methods present variations of the original data instead of producing new images and they provide limited improvement in model performance [8].

Recently, generative models such as generative adversarial networks (GANs) have emerged as promising methods for the data problem. GAN architecture, proposed by Ian Goodfellow et al. in 2014, generates fake data that resembles the real data distribution by creating a competitive learning process between two artificial neural networks, called as generator and discriminator networks [9]. This method is considered as a possible method that can provide data diversity without being constrained by ethical limitations [10], especially in sensitive areas such as medical imaging [11].

In addition, synthetic data plays an important role in protecting data privacy [12]. These artificial samples eliminate the risk of leaking sensitive personal information. In fact, a study published by the Allen Turing Institute in 2022 emphasized that synthetic data should be one of the essential tools in developing privacy-focused artificial intelligence systems [13].

Current brain tumor classification systems have several challenges, such as:

- Limited availability and privacy of medical imaging data: the performance of deep learning models strongly depends on the availability of large, diverse, and well-labeled datasets. However, obtaining real brain MRI data is challenging due to ethical restrictions, patient privacy concerns, and institutional limitations.

• Data imbalance and limited generalization: public brain MRI datasets often suffer from class imbalance. This leads to models that generalize poorly in clinical practice.

• Inability to share data across institutions: due to strict data protection regulations (e.g., HIPAA, GDPR), data sharing between institutions is almost impossible. This leads to the development of isolated models with limited robustness and external validity.

In order to overcome these challenges, this paper proposes some solutions listed below:

• GAN-based synthetic MRI image generation: We propose a framework that uses a GAN architecture (LS-WGAN-GP) to generate diverse and realistic synthetic brain MRI images. This allows the training of deep learning classifiers on enriched datasets without exposing real patient data.

• Augmented training with synthetic and real data: By combining real and GAN-generated images into an augmented dataset, the proposed framework improves class balance, enhances model generalization, and reduces overfitting. This also enables performance enhancement without needing to access private data.

• Privacy-preserving model training via synthetic data: Since the synthetic images are not linked to any real patient identity, the use of such data enables privacy-friendly model development.

Although the Br35H dataset used in this study is publicly available and anonymized, it serves as a benchmark dataset for evaluating the feasibility of synthetic-data-driven learning. Therefore, the present work should be interpreted as a proof-of-concept investigation that simulates privacy-constrained medical imaging environments, where direct access to patient data is often restricted. The objective is not to address an existing privacy issue within the dataset itself, but rather to assess whether synthetic MRI images can function as an alternative training resource in future privacy-sensitive clinical applications.

The main contributions of the study are given as follows:

• We present a GAN-based brain MRI augmentation and synthetic-data evaluation framework that enables systematic comparison of real, synthetic, and hybrid training scenarios for brain tumor classification. The framework allows training with synthetic or hybrid datasets and improves model robustness under data-constrained settings.

• We present a multi-model evaluation strategy using state-of-the-art transfer learning architectures to benchmark classification performance across real, synthetic, and hybrid datasets. This provides clear insights into model sensitivity and reliability under different data regimes.

• We explore synthetic-only training as a proof-of-concept approach for privacy-sensitive medical imaging scenarios. One contribution of this work is the comprehensive evaluation of synthetic-only training within the Br35H dataset and its comparison against real-data and hybrid-data training strategies.

In this study, we generated synthetic brain MRI images using a GAN-based architecture and compared the classification capabilities of transfer learning models trained on these images. We also analyzed the effects of augmented datasets created by combining both data sources (original and synthetic) on model generalization. This setup extends previous research by systematically comparing real-data, synthetic-data, and hybrid-data training strategies a publicly available tumor dataset using multiple transfer learning architectures.

2. RELATED WORKS

Creating synthetic brain MRI images with the GAN architecture is both a necessary and challenging task [14]. Han et al. [15] generated highly realistic images using DCGAN [16] and WGAN

[17], which were evaluated by an expert physician through a Visual Turing test [18]. In particular, these two models have demonstrated strong potential in some applications such as data augmentation and medical training because of their ability to produce highly realistic synthetic images.

Similarly, various GAN architectures including Pix2Pix, CycleGAN, DiscoGAN, and AttentionGAN have been employed to generate synthetic PAPSMEAR datasets, with their performances evaluated comparatively. In addition, a novel architecture, Pix2PixSSIM, was proposed by incorporating the structural similarity index, providing promising results in terms of image quality and performance [19].

GAN-based approaches to generate synthetic MR images for brain anomaly detection was proposed by Raja et al. [20]. In the experimental studies, their findings showed that the proposed model outperformed existing methods with 99% accuracy and 98% F1-score.

Synthetic MRI images from T1-weighted datasets using DCGAN was generated by Kazuhiro et al. [21]. The generated images were assessed by five radiologists, who confirmed their suitability for expanding training datasets.

Güvenç et al. addressed data scarcity in medical imaging and evaluated the effectiveness of similarity metrics for GAN-generated MR images. Their results showed that PSNR was not suitable for this purpose, while MSE and SSIM provided more reliable criteria for selecting synthetic images [22].

Andrio et al. generated synthetic brain MRI images using DCGAN and trained a ResNetV2 model, achieving high performance with 99.09% accuracy and 99.51% AUC. The study emphasized that DCGAN-generated images were more realistic than those produced by VanillaGAN [23].

Mehrotra et al. demonstrated that increasing dataset size through augmentation significantly improves classification performance. Using a dataset of 225×225 JPEG images, they achieved 99.04% accuracy with the AlexNet model despite limited data diversity [24].

Jiang et al. emphasized that synthetic datasets can be useful in clinical challenges involving large populations and in epidemiological events. They demonstrated that the use of synthetic datasets increased the data volume to overcome the data insufficiency in image processing studies conducted during the COVID-19 pandemic, thus effectively solving data scarcity problems [25].

In the study conducted by Taş et al., synthetic datasets based on computed tomography images were created for the classification of COVID-19 patients in a population consisting of normal and sick individuals. Based on the findings obtained as a result of this study, it was observed that the use of synthetic datasets could increase the accuracy of the process in the detection of nine diseases compared to the original datasets [26].

Loong et al. examined the use of synthetic data as a proxy for real-world data in large-scale health studies. The study examined inferential methods for synthetic data, including the selection of high-risk-of-disclosure variables for synthesis, the determination of prediction models, and the definition of disclosure risk assessment. The results showed that synthetic data can be used to allow researchers to conduct analyses while protecting patient privacy [27].

According to the studies existing in the literature, it is clear that GAN-based synthetic data generation methods are an important approach, especially for addressing privacy concerns and mitigating data insufficiency. Studies using different GAN architectures have yielded remarkable results in terms of both image quality and classification performance. In addition, these studies show the growing potential of GAN-generated synthetic data for both addressing data scarcity problem and supporting privacy-aware medical AI research. However, the effectiveness of synthetic data remains highly dependent on the dataset, generation method, and learning task. Therefore, further evaluation across different datasets and experimental settings remains necessary.

3. MATERIALS AND METHODS

This section gives some information about the data sets, tools, and systems developed and used in this study.

3.1. Brain MRI Data Sets

A comprehensive review was conducted to identify the dataset. As shown in Table 1, there are many datasets used in the diagnosis of brain tumors. In this study, the Br35H dataset was used to objectively evaluate model performance and test the generalizability of the proposed synthetic data generation approach due to its structural differences, diversity, and proximity to real-world conditions.

The Br35H dataset is a two-class classification dataset [28]. This feature allows testing the effectiveness of the proposed method on simple datasets in a test environment where real-synthetic comparisons can be directly observed [29]. This dataset also presents a suitable scenario for observing the effect of GAN-based data augmentation methods in data-insufficient conditions due to the limited number of samples it contains. Figure 1 and Figure 2 show examples from the Br35H dataset.

Figure 1. BR35H Dataset Non-tumor MRI images

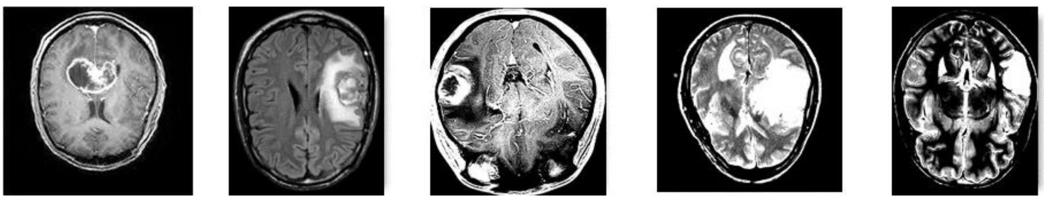

Figure 2. BR35H Dataset Tumor MR images

Table 1. Brain MRI data sets available in the literature

Data set	Source	Purpose	Image Type	Current Sequences	Number of Images	Number of Patients	Works Used
Br35H	Kaggle	Brain tumor segmentation	Normal, Tumor	T1, T2	3000	-	[28], [29]
BraTS 2012	MICCAI 2012 Competition	Brain tumor segmentation	GBM (LGG, HGG)	T1, T1c, T2, FLAIR	35 E 15 T	45	[30], [31]
BraTS 2013	MICCAI 2013 Competition	Brain tumor segmentation	GBM (LGG, HGG)	T1, T1c, T2, FLAIR	35 E 25 T	65	[32], [33]
BraTS 2014	MICCAI 2014 Competition	Brain tumor segmentation	GBM (LGG, HGG)	T1, T1c, T2, FLAIR	200 E 38 T	50	[32], [34]
BraTS 2015	MICCAI 2015 Competition	Brain tumor segmentation	GBM (LGG, HGG)	T1, T1c, T2, FLAIR	-	253	[35], [36]
BraTS 2016	MICCAI 2016 Competition	Brain tumor segmentation	GBM (LGG, HGG)	T1, T1c, T2, FLAIR	200 E 191T	391	[36], [37]
BraTS 2017	MICCAI 2017 Competition	Brain tumor segmentation	GBM (LGG, HGG)	T1, T1c, T2, FLAIR	285 E 146T 46 D	477	[35], [34]
BraTS 2018	MICCAI 2018 Competition	Brain tumor segmentation	GBM (LGG, HGG)	T1, T1c, T2, FLAIR	285 E 146T 55 D	542	[38], [39]
BraTS 2019	MICCAI 2019 Competition	Brain tumor segmentation	GBM (LGG, HGG)	T1, T1Gd T2, T2-Flair	-	259 HGG 76 LGG	[40], [41]
Brain Web	McConnell Brain Imaging Center	Providing realistic brain MRI images	Normal, MS	T1, T1c, T2,	201	11	[42], [43]
AANLIB	Harvard Medical School	Detection of brain abnormalities	Normal, Tumor	T1, T2	-	-	[44], [45]
Cjdata	School of Biomedical Engineering, Guangzhou, China	Brain tumor classification	Meningioma Glioma Pituitary Tumors	T1c	708, 1426, 930	233	[46], [47]
RIDER	TCIA	Treatment outcome assessment	Normal, Tumor	T1, T2	368	19	[48], [49]
ADNI	Alzheimer Disease Neuroimaging Initiative public-private partnership	Measuring the progression of mild cognitive impairment and early Alzheimer's disease	MCI, AD	T1	3416	3.416	[50], [51]
ABIDE I (2012)	University of California, Los Angeles and Pittsburgh School of Medicine	Individuals with and without autism spectrum disorder	fMRI	T1, T2, EPI	1112	539 ASD and 573 control subjects	[52], [53]
ABIDE II (2016)	University of California, Los Angeles and University of Pittsburgh School of Medicine	Individuals with and without autism spectrum disorder	fMRI	T1, T2, EPI	1114	521 ASD and 593 control subjects	[52], [53]
CE-MRI	Nanfang and Tianjin Medical Hospitals in China	Brain tumor classification	meningioma, glioma, and pituitary tumor	T1	3064	233	[54], [55]
Rembrandt	Open access dataset compiled by the National Cancer Institute	Major brain cancer studies	Normal, Glioma	T1, T2	671	671	[56], [57]
GAZI BRAIN	Gazi University	Detection of brain tumors	Normal, Glioma	T1, T2	100	100	[58], [59]

The BR35H dataset consists of three folders: yes, no, and pred. The yes folder contains 1500 brain MRI images with tumors, the no folder contains 1500 brain MRI images without tumors, and the pred folder contains 60 brain MRI images. These images are in JPG format and their sizes vary.

3.2. Method

In this section, transfer learning methods, the metrics used, and the model framework developed in this study are presented.

Transfer learning aims to improve performance in a new task by leveraging the knowledge of a pre-trained model. A pre-trained model is a machine learning model that has been trained on a large dataset. The dataset used to train this model is usually much larger than the dataset that will be used to train the model for classification. The pre-trained model learns to extract features from the data, and these features can be used to train the model for classification more quickly and efficiently [60].

DenseNet201

The DenseNet architecture proposed by Huang et al. uses a simple connection pattern that directly connects all layers to each other in a feedforward manner. Each layer receives additional inputs from all previous layers and passes its feature maps to all subsequent layers. The main components that make up DenseNet are dense blocks and transition layers. The former defines how inputs and outputs are connected, while the latter controls the number of channels. DenseNet uses ResNet's modified batch normalization, activation, and convolution structure. With this architecture, DenseNet has various advantages, including mitigating the vanishing gradient problem, strengthening feature propagation, encouraging feature reuse, and significantly reducing the number of parameters. DenseNet algorithms can be used in different versions such as DenseNet121, DenseNet169, and DenseNet201, depending on the number of layers used [61].

Xception

The Xception model, which emerged with the further development of the Inception architecture by Google, is designed with a deeper and wider architecture than others. The model consists of three streams: input, middle, and output. After passing through the input stream, the data passes through the middle stream, which repeats eight times, and then reaches the output stream. Normalization operations are applied in all convolution layers in the Xception model [62].

VGG16 – VGG19

It is a deep learning model developed in 2014. It performed quite successfully in the ImageNet 2014 competition with an error rate of 7.3%. Designed by Simonyan and Zisserman at Oxford University, this architecture has produced six different architectures [63]. The VGG algorithm is named according to the number of layers used. For example, if a 16-layer structure is used, it is referred to as VGG16, and if a 19-layer architecture is used, it is referred to as VGG19. These transfer learning models are commonly found in the literature. VGG is known as an architecture that produces simple and efficient results. In the literature, it has been used in studies involving various tasks, including image classification, object detection, and segmentation, and has achieved good performance results [64].

InceptionResNetV2

The InceptionResNetV2 model is an effective and fast learning model developed by Google by combining the learning advantages of Inception architecture with Residual Networks. At the core of the model are parallel structures that enable complex features to be processed at multiple scales. This allows information of different sizes to be processed simultaneously. In addition, residual connections accelerate learning by reducing information loss between layers. This structure increases accuracy and prevents problems during the training process, especially with large data sets [65].

ResNet50

ResNet50 is a 50-layer residual network with 26 million parameters. It is a deep convolutional neural network model introduced by Microsoft in 2015 [66]. It is known for its ability to learn deeper features. Instead of learning features, a residual network learns residuals, which are the extraction of learned features from the input layers [67].

InceptionV3

An architecture developed by Google and recognized for its high performance among deep learning models. It has a modular structure that efficiently organizes complex information flows. This reduces information loss between layers while eliminating the challenges encountered in the learning processes of deeper architectures [68]. Thanks to factorized convolutions in particular, filters with large kernel sizes are divided into smaller and more computable filters. This allows the model to run faster and increases its learning capacity with less data [69].

NASNetMobile

It is an architecture developed using Neural Architecture Search (NAS), a method that enables the automatic design of deep learning models. The primary goal of this architecture is to provide a flexible model that delivers high accuracy while also functioning effectively on systems with limited resources, such as mobile devices [70]. One of the most notable features of NASNetMobile is its modular structure. This means that the model's basic building blocks are reusable and customizable. As a result, the same basic architecture can be easily adapted for tasks of different sizes [71]. As a result, the NASNetMobile architecture combines powerful performance and efficiency to deliver effective solutions for applications running on limited resources.

EfficientNetV2B0

EfficientNetV2B0 is a deep learning architecture developed by Google researchers and is the latest member of the EfficientNet family. This architecture is designed for image classification and other visual tasks, aiming to provide a faster and more effective solution. It retains all the advantages of the EfficientNet architecture while introducing improvements that further enhance performance. EfficientNetV2B0 can be run efficiently not only on mobile devices with limited hardware resources but also in large-scale data centers [72]. EfficientNetV2B0 achieves very high accuracy despite being small and compact.

ConvNeXtTiny

It is the smallest and most optimized member of the ConvNeXt family, which performs well in deep learning-based image processing tasks. The ConvNeXt architecture offers a design that modernizes the CNN approach and delivers competitive performance against new-generation architectures such as Vision Transformers (ViT). Due to its small size and optimized architecture, ConvNeXtTiny can operate with low latency and energy consumption. It stands out for its superior performance in tasks such as image classification, object detection, and segmentation [73].

3.3. Evaluation Metrics

Different metrics are used to measure the performance of transfer learning classification models. The metrics and their characteristics used to evaluate the performance of the models in our study are described below [77].

Accuracy: It is the ratio of examples that the model predicts correctly. The maximum value of accuracy can be 100.

Recall: It shows how many of the true positive examples are classified as positive.

Precision: It shows how many of the samples classified as positive are actually positive. Precision measures the model's ability to correctly classify the positive class.

F1score: The F1 score is the harmonic mean of the Precision and Recall scores. It is useful for achieving a balance between precision and recall by balancing these two metrics into a single number.

Specificity: is the proportion of samples that are truly negative that yield a negative result in a test.

3.4. Generation of Synthetic Data

As the need for data to train models increases, so do concerns about data privacy. Using data without the permission of the data owners is illegal. One of the methods used to strike a balance between privacy and benefit is to generate synthetic data. The synthetic data production method, which captures most of the complexity in original datasets that do not contain any clues from real data and minimizes the risk of data identification, is considered a reasonable solution [74]. GAN technology is a cutting-edge technology that enables the generation of artificial data without compromising user privacy. Table 2 presents some GAN models developed for specific purposes.

A review of the literature revealed that DCGAN and WGAN models perform well in medical image generation. The chosen GAN model should avoid mode collapse and be capable of generating high-resolution, realistic MR images.

Table 2. GAN models used in some applications in the field of medicine and health in the literature [75]

Medical and Health Application	**GAN Models**
Image-to-image translation	pix2pix, CycleGAN, MR-GAN, MCMLGANs, Tub-GAN and Tub-sGAN, MedGAN, DermGAN
Synthetic image generation	WGAN, WGAN-GP, DCGAN, BEGAN, ProGAN, fNIRS-GANs, ACGAN
Image configuration	SRCNN, VDSR, DRCN, ESRGAN, mDCSRN-GAN, MedSRGAN

3.5. Synthetic Data Generation Model – LS-WGAN-GP

Two network models, a Discriminator Network and a Generator Network, are used; the discriminator network replaces the classic DCGAN discriminator to avoid mode-collapse artifacts and improve convergence. This type of GAN uses the Wasserstein distance and critic loss to distinguish real and fake data. Furthermore, a gradient penalty is applied to the weights, allowing the function to satisfy the K-Lipschitz constraint. The goal of the critic loss is to converge to 0 to reach the minimum difference between fake and real images. Since the discriminator cannot distinguish between 0 and 1 in binary terms, the Sigmoid function and binary cross-entropy loss were deleted in this case, and the model was named Critic instead of Discriminator. An LS-GAN was used as the generator to achieve high-quality performance. Otherwise, it was penalized using the WGAN. In this case, the MSE loss is backpropagated from the generator for real and fake samples [76].

Discriminator Network: The discriminator consists of three blocks. Each block contains a convolutional filter, a sample normalization layer, and a Leaky ReLU activation function. The model takes as input a tensor of the form [16 (groups) x 1 (channel) x 64 (H) x 64 (W)] from the generator and the embedding condition represented by the label. These are passed through the first kernel to generate 64 feature maps using a 4-dimensional kernel with a 2-stride, thus reducing the spatial dimensions. The first block takes 64 features and generates 128 feature maps with the same kernel size and stride. The second block does the same and generates 256 feature maps. The third block generates 512 feature maps. Finally, the embedding layer allows the model to concatenate the label vector to the image, enabling it to classify images conditioned on the label vector.

Generator Network: The generator network consists of 5 blocks. Each block consists of a transposed convolution layer, a batch normalization layer, and ReLU as the activation function. It starts with random noise of size [groups x 128 x 1 x 1]. The first block takes 256 features (from the noise + the size of the embedding to be combined during the forward pass) and produces 1024 features with a kernel of size 4, stride of 1, and padding of 0 (since we do not want to reduce the spatial dimensions in this section). The second block takes 1024 features and produces 512 features. The third block produces 256 features. The fourth block produces 128 features. The fifth block produces 64 features. The final layer is a transposed convolutional layer that takes 128 fields as inputs and produces 1 output, which will generate a hyperbolic tangent activation function. The output will be a 3 x 128 x 128 image.

A 128x128 resolution was used to reduce GPU memory consumption and enable stable GAN training within the computational constraints of the Google Colab Pro environment.

3.6. Programming

The experiments were conducted in the Google Colab Pro environment using an NVIDIA T4 GPU. Python 3.10 was used as the programming language. The following Python libraries were employed during model development, training, evaluation, and visualization: PyTorch, Torchvision, TorchMetrics, NumPy, Pandas, Matplotlib, Seaborn, Pillow, and Scikit-learn.

3.7. Preprocessing

Prior to GAN training, the MRI images were randomly divided into training (80%) and validation (20%) subsets. All images were resized to 128×128 pixels, converted into tensor format, and normalized to the range of [-1, 1] using a mean value of 0.5 and a standard deviation of 0.5 for each RGB channel. No data augmentation techniques were applied during GAN training.

For the transfer learning stage, all images were resized to 224×224 pixels to satisfy the input size requirements of the pre-trained architectures. Pixel values were rescaled to the range of [0, 1] using a normalization factor of 1/255. In addition, 10% of the training data was reserved for validation using the validation_split parameter. No data augmentation operations, such as rotation, flipping, shifting, or zooming, were applied during classifier training. To ensure a fair comparison among the transfer learning architectures, the same training, validation, and test partitions were used in all experiments.

4. MODEL DEVELOPMENT FOR BRAIN MRI CLASSIFICATION

4.1. Generating Synthetic Images with LS-WGAN-GP

To generate synthetic brain MR images, two network models—a discriminative network and a generative network—are trained because of the nature of GAN technology.

For the discriminative network, a gradient-penalized Wasserstein GAN is used instead of the classical DCGAN to prevent mode collapse and improve convergence. This type of GAN uses the Wasserstein distance and critic loss to distinguish between real and spurious images. Then, a gradient penalty is applied to the weights, allowing the function to satisfy the K-Lipschitz constraint. The purpose of the critic loss is to converge to 0 to achieve the minimum difference between spurious and real images. Since the discriminative network will not distinguish between 0 and 1 in terms of binary discrimination, the discriminative model created by removing the sigmoid function and binary cross-entropy loss is called the critic. For the generative network, an LSGAN is used, which provides high-quality images. Otherwise, it is penalized by using a WGAN. In this case, the MSE loss is propagated back from the generator to compare the real and fake images.

In this section, we generated synthetic brain MRI images using the LS-WGAN-GP model. The hyperparameters used in the data generation process are explained in Table 3. In addition, a gradient penalty is applied to the critic loss of the discriminator as a regularization technique that improves image quality and diversity by preventing mode collapse. Adam was chosen as the optimizer for both the generator and the discriminator (critic); for the generator, the learning rate is 0.0002, beta1 is 0.5, and beta2 is 0.99, while for the discriminator, the learning rate is 0.0001, beta1 is 0, and beta2 is 0.9. Figures 3 and 4 present examples of synthetic datasets with non-tumor and tumor cases.

Table 3. Hyperparameters and descriptions

Parameter	Value	Description
img_size	128	The size of the generated images is set to 128x128 pixels
channels_img	3	The images are specified to have three color channels (RGB)
gen_embedding	128	The size of the embedding layer used in the generator model
z_dim	128	The size of the random noise vector that the generator receives as input
num_epochs	500	The number of epochs to be run during the model's training process
lambda_gp	10	The coefficient used for Gradient Penalty
features_d	64	The number of basic filters used in the discriminator model
features_g	64	The number of basic filters used in the generator model
critic_iter	3	The number of times the discriminator will be updated for each generator update

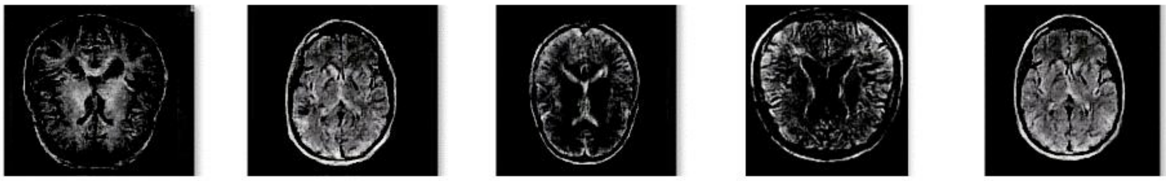

Figure 3. Synthetic dataset samples generated using BR35H Dataset (Non-tumor MRI images)

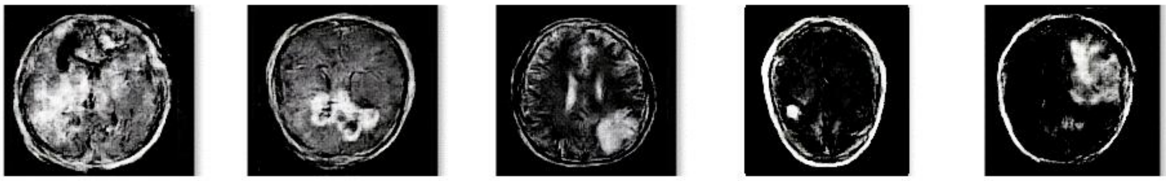

Figure 4. Synthetic dataset samples generated using BR35H Dataset (Tumor MRI images)

The model generated 500 new synthetic images with tumors and 500 without tumors. FID and Inception Score were calculated for the entire set and compared with the same number of synthetic images to obtain an overview. The FID score, comparing the distribution of real and fake images, was 144.94 and the Inception Score, comparing the diversity and difference in the dataset, was 1.4731 out of 2, with a standard deviation of 0.1429. When the obtained Inception score, standard deviation, and FID scores are evaluated together, they provide results consistent with the goal of using synthetic data not for direct diagnostic purposes, but in the context of data augmentation and model training while protecting privacy.

4.2 Modelling for Classification

In this study, a classification process using transfer learning-based methods was implemented to examine the usability of synthetically generated data in place of real data in the classification of brain tumor image-based data. In the classification approach, the preprocessing of the data was carried out. The data were divided into three groups as training, validation, and testing. Transfer learning models were developed. These models were trained and subsequently tested. Performance analysis of the results was then conducted in Section 4. This main framework is outlined in Figure 5.

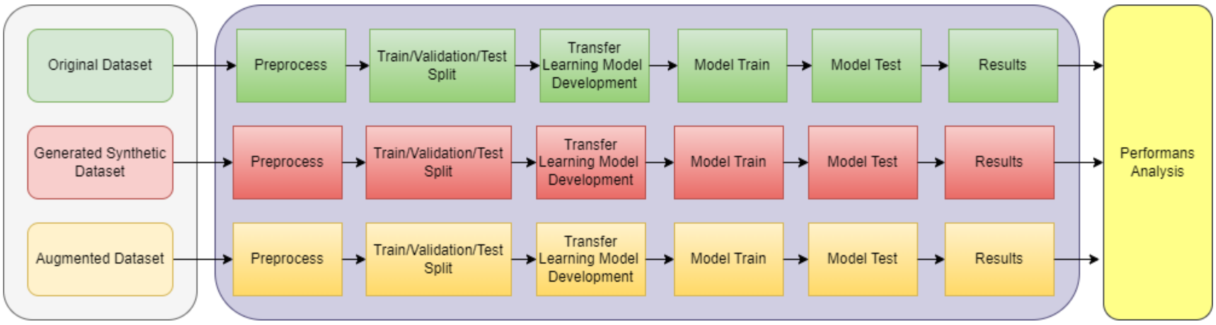

Figure 5. Classification framework

The BR35H dataset was used in the experiments. Synthetic data generation processes were also performed for the dataset. The data were preprocessed in accordance with the classification models. The dataset used contains a total of 1500 images with tumors and 1500 images without tumors. 200 of each were selected as test data. 20% of the 1300 images with tumors and 1300 images without tumors were randomly selected as validation data.

Since the transfer learning architectures used in this study require an input size of 224×224 pixels, the generated 128×128 synthetic MRI images were resized to 224×224 prior to model training. The resizing process was performed using nearest-neighbor interpolation, which corresponds to the default interpolation method implemented in the Keras ImageDataGenerator framework. This approach was adopted to ensure compatibility with the pre-trained network architectures while preserving the original image content.

Synthetic brain MRI images were generated using the WGAN-GP architecture for tumor and non-tumor classification, and compared with the real dataset. These images were subjected to a quality control process and included in the classification phase. The synthetic images generated were intended not only to increase the data volume, but also to evaluate the effect of privacy-preserving data on classification performance. Three different scenarios were considered in the classification process. First, the data consisted only of real data; then, only synthetic data were used. Finally, a scenario combining both datasets was examined.

The hold-out validation method was chosen due to the substantial computational cost associated with repeatedly training multiple GAN and transfer learning models under a k-fold cross-validation framework. Considering the available computational resources and training time requirements, the hold-out approach provided a practical and efficient evaluation strategy. Nevertheless, k-fold cross-validation may offer a more robust assessment of model generalizability and can be considered in future studies.

Each scenario was subjected to its own training and testing processes, and the obtained results were compared. In the modeling process, pre-trained deep learning architectures frequently used in medical images, such as DenseNet201, Xception, VGG16, VGG19, InceptionResNetV2, ResNet50, InceptionV3, NASNetMobile, EfficientNetV2B0, and ConvNeXtTiny were used. The upper layers of these models were customized to accommodate binary classification of brain tumor presence or absence, and all models were trained with the same hyperparameters given in Table 4.

Table 4. Hyperparameters and descriptions used in transfer learning models

Parameter	**Value**	**Description**
Optimizer	Adam	Compiled using Adam optimizer (1e-5)
Batch	64	The number of images processed simultaneously by the model (batch size) is set to 64.
Epoch	20	For each model, the create_model function was called and trained for 20 epochs with the training and validation datasets.
Loss function	Binary crossentropy	Binary cross entropy was preferred as the loss function.

5. EXPERIMENTAL STUDIES AND RESULTS

Experimental studies have investigated whether classification models can be trained with synthetic data and perform with high accuracy without access to real patient data. The results are presented below.

The BR35H dataset has a balanced distribution and contains brain images with and without tumors. High-quality synthetic data were generated using the GAN-based architecture. These data were used for both data augmentation and fully synthetic training scenarios in the classification models. Experiments were performed using pre-trained weights in transfer learning models. The classification performances of real, synthetic, and augmented datasets were analyzed comparatively during the training and testing processes. The results of these analyses are presented in Table 5 and Figures 6, 7, and 8.

Table 5. Performance of transfer learning classifiers on BR35H dataset (original, synthetic, and augmented)

Model	Dataset	Accuracy	Precision	Recall	F1score	Specificity
DenseNet201	Original	0.9150	0.9246	0.9150	0.9145	0.9246
	Synthetic	0.9600	0.9613	0.9600	0.9600	0.9613
	Augmented	0.9140	0.9213	0.9140	0.9136	0.9213
Xception	Original	0.9500	0.9537	0.9500	0.9499	0.9537
	Synthetic	0.9533	0.9554	0.9533	0.9533	0.9554
	Augmented	0.9260	0.9318	0.9260	0.9258	0.9318
VGG19	Original	0.8700	0.8810	0.8700	0.8691	0.8810
	Synthetic	0.8600	0.8616	0.8600	0.8598	0.8616
	Augmented	0.8560	0.8827	0.8560	0.8534	0.8827
InceptionResNetV2	Original	0.9300	0.9386	0.9300	0.9297	0.9386
	Synthetic	0.9533	0.9534	0.9533	0.9533	0.9534
	Augmented	0.9420	0.9436	0.9420	0.9419	0.9436
ResNet50	Original	0.6925	0.6925	0.6925	0.6925	0.6925
	Synthetic	0.8000	0.8002	0.8000	0.8000	0.8002
	Augmented	0.7280	0.7281	0.7280	0.7280	0.7281
InceptionV3	Original	0.9275	0.9354	0.9275	0.9272	0.9354
	Synthetic	0.9533	0.9541	0.9533	0.9533	0.9541
	Augmented	0.9240	0.9330	0.9240	0.9236	0.9330
NASNetMobile	Original	0.8900	0.9062	0.8900	0.8889	0.9062
	Synthetic	0.9467	0.9479	0.9467	0.9466	0.9479
	Augmented	0.9240	0.9279	0.9240	0.9238	0.9279
EfficientNetV2B0	Original	0.5800	0.6166	0.5800	0.5443	0.6166
	Synthetic	0.5333	0.5534	0.5333	0.4849	0.5534
	Augmented	0.5780	0.6382	0.5780	0.5264	0.6382
VGG16	Original	0.8700	0.8824	0.8700	0.8689	0.8824
	Synthetic	0.8733	0.8739	0.8733	0.8733	0.8739
	Augmented	0.8640	0.8792	0.8640	0.8626	0.8792
ConvNeXtTiny	Original	0.8325	0.8387	0.8325	0.8317	0.8387
	Synthetic	0.8200	0.8228	0.8200	0.8196	0.8228
	Augmented	0.7960	0.8379	0.7960	0.7895	0.8379

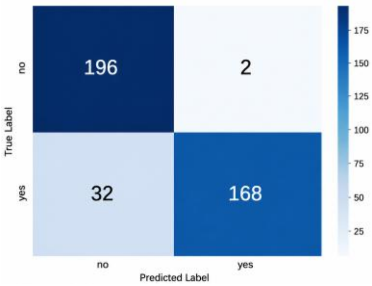

a) DenseNet201

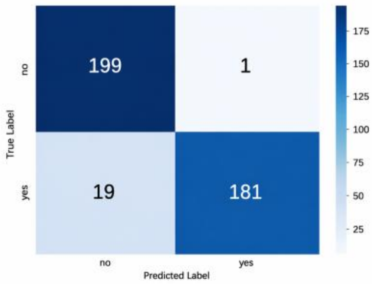

b) Xception

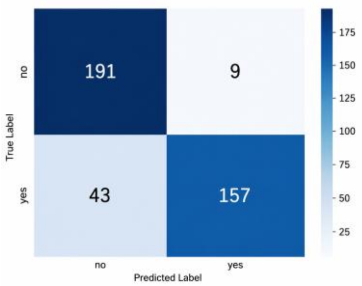

c) VGG19

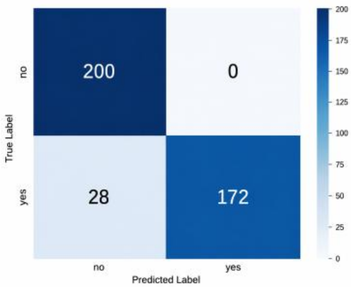

d) InceptionResNetV2

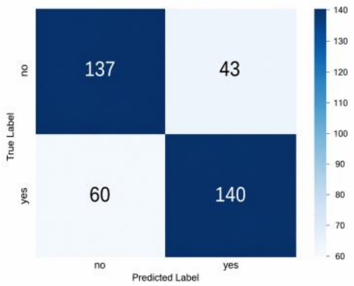

e) ResNet50

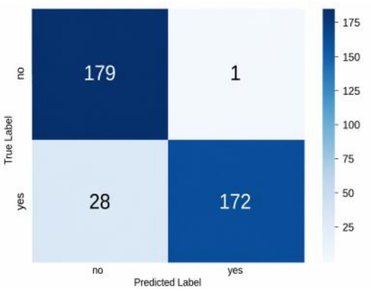

f) InceptionV3

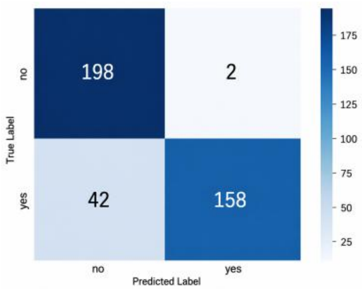

g) NASNetMobile

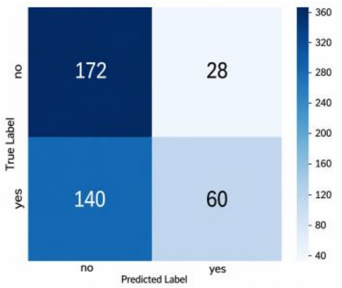

h) EfficientNetV2B0

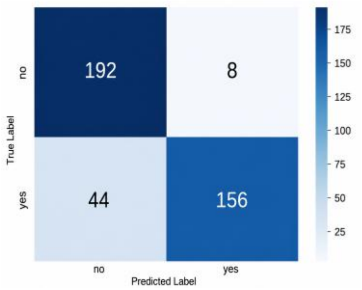

i) VGG16

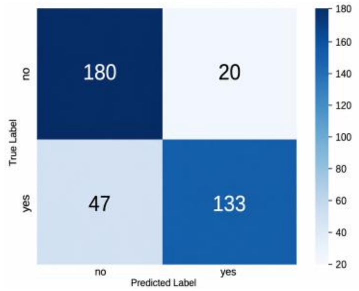

j) ConvNeXtTiny

Figure 6. Confusion matrix of models (original dataset)

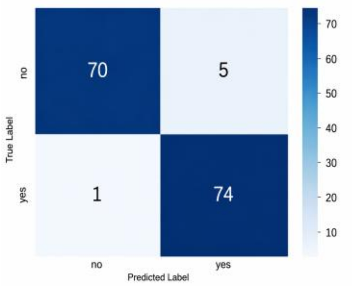

a) DenseNet201

b) Xception

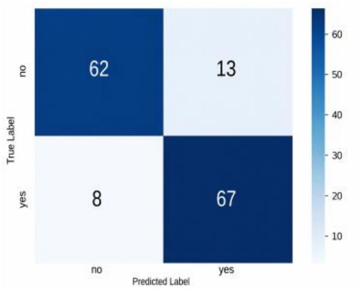

c) VGG19

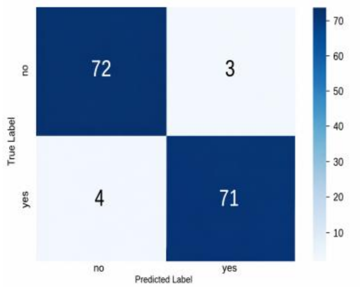

d) InceptionResNetV2

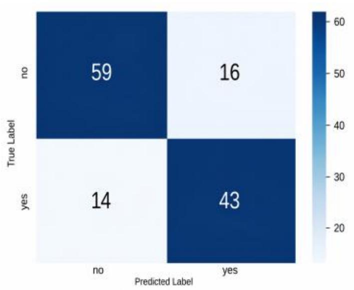

e) ResNet50

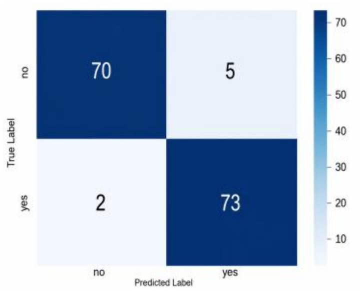

f) InceptionV3

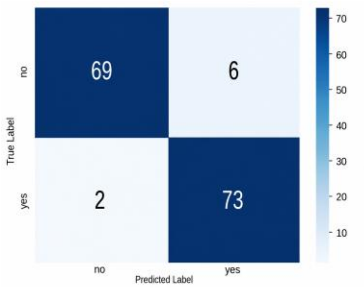

g) NASNetMobile

h) EfficientNetV2B0

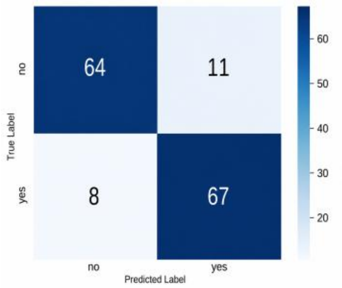

i) VGG16

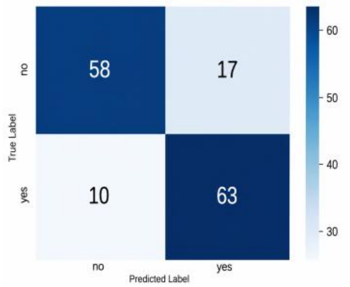

j) ConvNeXtTiny

Figure 7. Confusion matrix of models (synthetic dataset)

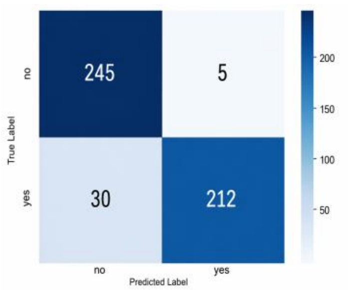

a) DenseNet201

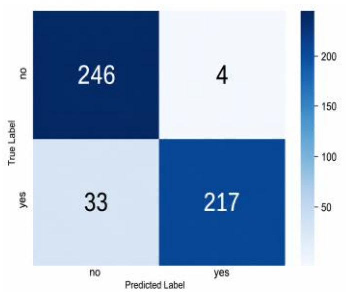

b) Xception

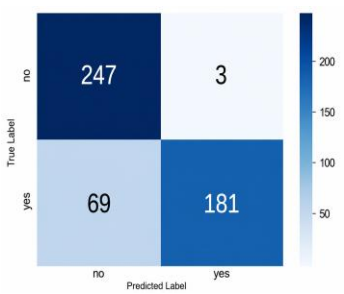

c) VGG19

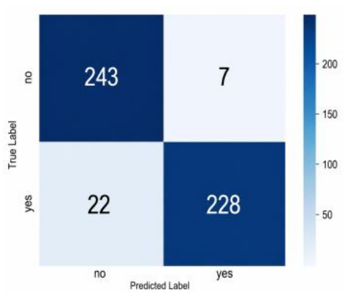

d) InceptionResNetV2

e) ResNet50

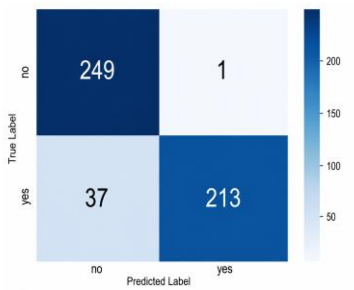

f) InceptionV3

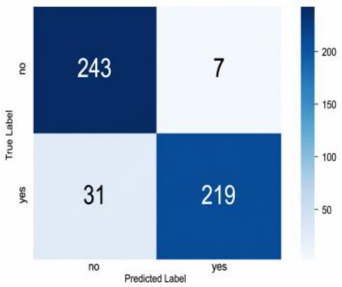

g) NASNetMobile

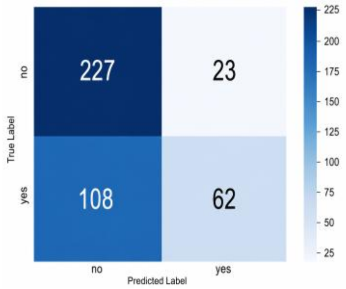

h) EfficientNetV2B0

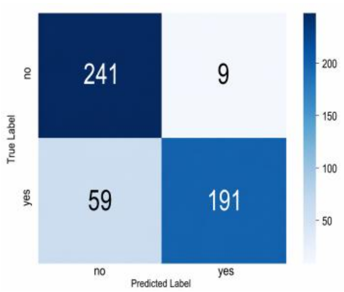

i) VGG16

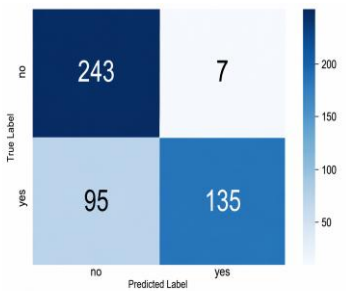

j) ConvNeXtTiny

Figure 8. Confusion matrix of models (augmented dataset)

The precision, recall, and F1-score values presented in Table 5 were calculated using the weighted average option (`average='weighted'`) of the Scikit-learn metric functions. Therefore, these values are not directly equivalent to metrics manually calculated from the positive class entries of the confusion matrix.

Experiments with the BR35H dataset have yielded significant results in terms of evaluating the impact of synthetic data on classification success. It has been determined that models trained solely on synthetic data offer comparable accuracy to real data in some transfer learning algorithms. In particular, the Xception model achieved 95% accuracy with the real dataset, while achieving a high success rate of 95.33% with only synthetic data and 92.6% with augmented data. This result demonstrates that GAN-based generation is an effective alternative for protecting data privacy. On the other hand, the use of augmented data provides limited increases in overall accuracy in some models. This situation shows that the direct contribution of synthetic data to the used dataset may be limited, but it has high potential in terms of data diversity.

6. EXPLAINABILITY ANALYSIS USING GRAD-CAM

To demonstrate the explainability of the deep learning models used in this study and to provide insight into their decision-making process, Gradient-weighted Class Activation Mapping (Grad-CAM) was applied to representative MRI images. As an illustrative example, Figures 9-12 present Grad-CAM visualizations obtained from the DenseNet201 model trained on the synthetic dataset and original dataset.

Figures 9-12 present Grad-CAM visualizations obtained from the DenseNet201 model trained on synthetic brain MRI images. To provide a comprehensive interpretation of the model's decision-making process, Grad-CAM maps are shown for both tumor and non-tumor cases from the synthetic dataset as well as from the original dataset. The images show that the model perfectly focuses on anatomically meaningful intracranial regions when performing classification. For tumor-positive cases, the activation maps are concentrated around the lesion-related areas and surrounding tissue structures. This indicates that the model utilizes relevant pathological characteristics associated with tumor presence. In contrast, for non-tumor cases, the attention regions are distributed across normal brain structures without emphasizing localized abnormal patterns, which is consistent with the absence of tumor-related findings.

Importantly, the activation maps do not exhibit substantial attention toward image borders, background regions, or visually irrelevant patterns that could potentially arise from the image generation process. This observation suggests that the DenseNet201 model has learned clinically meaningful anatomical representations rather than relying on synthetic generation artifacts. Furthermore, the similar attention patterns observed in both synthetic and original MRI samples indicate that the features learned from synthetic data are transferable to real-world images and correspond to relevant anatomical structures.

The Grad-CAM analysis highlights that the used deep learning framework is interpretable and capable of identifying clinically relevant regions associated with tumor presence. This supports the overall reliability of the proposed approach and provides additional evidence that the learned representations are based on meaningful diagnostic characteristics.

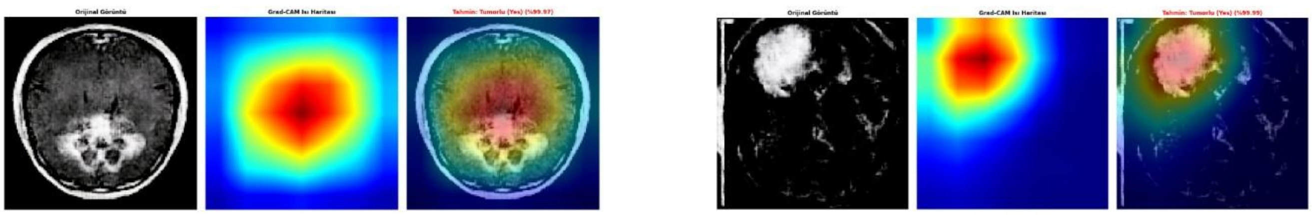

Figure 9. Tumor samples (Synthetic dataset)

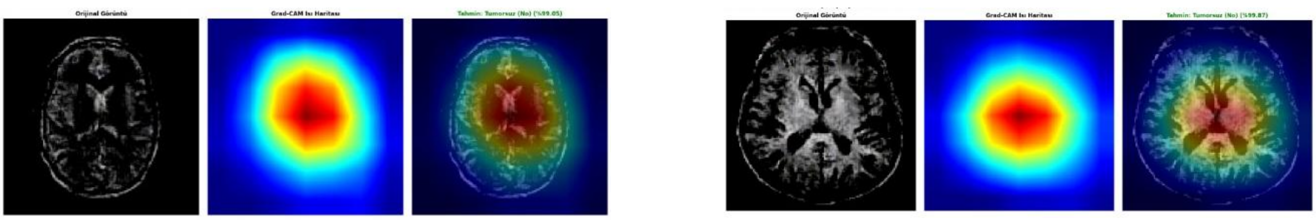

Figure 10. No-tumor samples (Synthetic dataset)

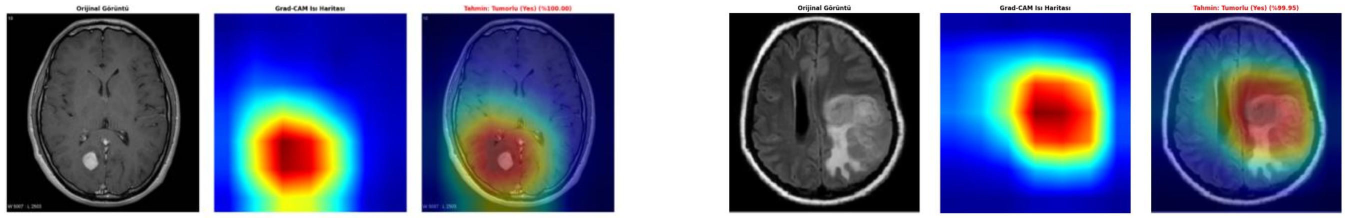

Figure 11. Tumor samples (Original dataset)

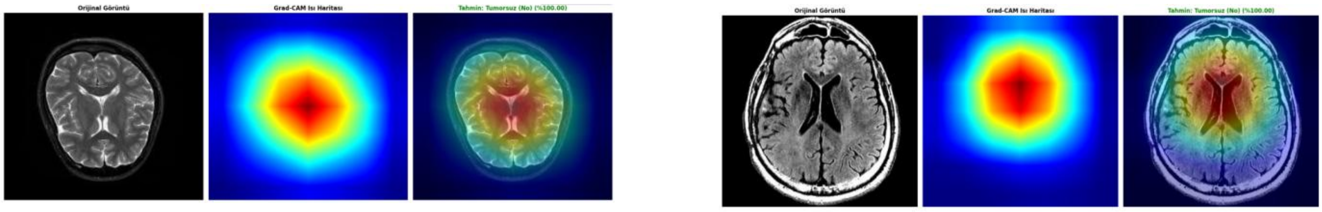

Figure 12. No-tumor samples (Original dataset)

7. DISCUSSION

This study proposes a framework that tests the usability of synthetic images generated with GAN instead of real brain MRI images in classification processes. When the obtained results are examined;

• The results obtained with the DenseNet201, Xception, InceptionResNetV2, and InceptionV3 models are particularly noteworthy. In these models, metrics such as accuracy, precision, recall, F1 score, and specificity obtained using the synthetic dataset were often higher than those obtained using the original dataset.

• For example, with the DenseNet201 model, an accuracy of 96% was achieved with synthetic data, while this rate remained at 91.50% with the original data set. However, the accuracy obtained with the augmented data set is slightly lower (91.40%). This suggests that synthetic data provides a more significant contribution when used alone, but this effect may be slightly reduced in augmented datasets.

• A similar situation was observed in the Xception model. An accuracy of 95.33% was achieved with synthetic data, which is higher than the original data. In contrast, the accuracy dropped to 92.60% in the augmented dataset.

• Interestingly, the InceptionResNetV2 model showed the highest performance with synthetic data. In this model, results above 95% were obtained in all metrics, such as F1 score, precision, and recall. Similarly, balanced results were obtained with the augmented dataset.

The results indicate that augmented dataset does not consistently improve performance and may even lead to slight decreases in some models. This can be attributed to the distribution mismatch between real and GAN-generated images, where synthetic samples may contain subtle artifacts or unrealistic patterns. Additionally, limited diversity or potential mode collapse in GAN-generated data may introduce redundancy rather than meaningful variation. The proportion of synthetic data is also critical; overrepresentation can bias models toward artificial features instead of clinically relevant structures. Furthermore, the impact is model-dependent, as some architectures are more robust to synthetic noise, while others are more sensitive to distribution shifts. These findings suggest that the effectiveness of GAN-based augmentation depends strongly on data quality, balance, and model robustness.

The performance differences observed among the transfer learning architectures may also be related to their structural characteristics and compatibility with the dataset. For instance, EfficientNetV2B0 exhibited lower performance compared to DenseNet201, Xception, and InceptionResNetV2. One possible explanation is that EfficientNet-based architectures are typically optimized for large-scale and highly diverse datasets, whereas the relatively limited size and homogeneous nature of the MRI dataset used in this study may restrict their ability to learn highly discriminative features. In addition, the distributional characteristics of GAN-generated images may not fully align with the feature extraction mechanisms of EfficientNetV2B0. Conversely, architectures such as DenseNet201 and Xception benefit from stronger feature reuse and more effective representation learning capabilities, enabling them to capture subtle tumor-related patterns more successfully in both original and synthetic datasets. These findings suggest that the effectiveness of synthetic data is not only dependent on data quality but also on the compatibility between the generated data and the underlying model architecture.

The experimental results show that models trained with augmented datasets achieve higher classification success compared to models trained solely with real data. This supports the positive contribution of GAN-based synthetic data, in particular, to model generalization capacity. The fact that models trained using only synthetic data can achieve high performance values indicates that such data will be an effective source not only for data augmentation but also for privacy-focused learning scenarios. This finding is critical, especially in medical artificial intelligence applications where the privacy of patients and their data must be protected. Furthermore, comparative analyses with transfer learning architectures such as Xception and DenseNet have shown that higher performance is achieved when hybrid data are used. These results demonstrate that transfer learning can operate with higher accuracy under data conditions close to the limit, and that success can be further increased if it is supported by synthetic data.

However, it has also been observed that models trained solely with synthetic data perform lower in some cases compared to models trained with real data. This shows that the quality of synthetic data has a direct impact on model performance and that the hyperparameters of the GAN architecture used in synthetic data generation should be carefully optimized. The findings provide additional evidence supporting the potential utility of GAN-generated synthetic MRI data for brain tumor classification and contribute to the growing body of research investigating synthetic data as a complementary or alternative training resource. In addition, by demonstrating that synthetic data can be used directly for model training, new research opportunities have been created in the field of medical image processing. In future studies, comparative analysis of different GAN architectures and the use of different synthetic data generation approaches should be evaluated to further increase the generalizability of the system.

One limitation of this study is that the dataset used includes a limited number of classes. The results obtained may differ when applied to datasets containing a broader range of tumor types, such as meningioma, glioma, and pituitary tumors. Therefore, the generalizability of the proposed approach to more diverse and multi-class datasets should be further investigated in future studies.

Although the Train on Synthetic, Test on Real (TSTR) protocol is commonly used in the literature to evaluate the statistical similarity between synthetic and real datasets, it was not included in this study because our research objective was different. Rather than focusing on how closely synthetic MRI images replicate the distribution of real scans, this study aims to explore the practical usefulness of synthetic data for privacy-preserving model development. In particular, we sought to examine whether synthetic images can serve as an alternative or supportive data source in real-world classification tasks. For this reason, the experimental design was based on three practical training scenarios: using only real data, only synthetic data, and a combination of both. This approach enables a more direct assessment of how synthetic data performs in classification settings and how much benefit it provides when integrated with real data.

Peer-review: External, Independent.

Acknowledgements:

The authors would like to thank all institutions and publicly available data sources that contributed to the development of the dataset used in this study. No additional acknowledgements are declared.

Declarations:

1. Statement of Originality:

The authors declare that this manuscript is original, has not been published previously, and is not under consideration for publication elsewhere. All sources, datasets, and references used in this study have been appropriately cited.

2. Author Contributions:

Concept: AS,YC; ***Conceptualization:*** AS,YC; ***Literature Search:*** AS,YC; ***Data Collection:*** AS,YC; ***Data Processing:*** AS,YC; ***Analysis:*** AS,YC; ***Writing – original draft:*** AS,YC; ***Writing – review & editing:*** AS,YC.

3. Ethics approval:

The dataset used in this research consists of publicly available and anonymized MRI images. The dataset does not contain any personally identifiable information and has been used in accordance with the terms and conditions of the relevant data source. Therefore, ethical committee approval was not required for this study.

4. Funding/Support:

The authors received no specific financial support, grant, or funding for this research.

5. Competing Interests:

The authors declare no competing interests.

6. GenAI Usage Statement:

No GenAI tools were used at any stage of the study.

7. Sustainable Development Goals:

✵ ✵ ✵

REFERENCES

[1] N. A. O. Bush, S. M. Chang, and M. S. Berger, "Current and future strategies for treatment of glioma," Neurosurgical Review, vol. 40, no. 1, pp. 1-14, 2017/01/01 2017.

[2] G. A. Amran et al., "Brain tumor classification and detection using hybrid deep tumor network," Electronics, vol. 11, no. 21, p. 3457, 2022.

[3] V. Dutoit, D. Migliorini, P.-Y. Dietrich, and P. R. Walker, "Immunotherapy of malignant tumors in the brain: how different from other sites?," Frontiers in oncology, vol. 6, p. 256, 2016.

[4] O. Ronneberger, P. Fischer, and T. Brox, "U-net: Convolutional networks for biomedical image segmentation," in Medical image computing and computer-assisted intervention–MICCAI 2015: 18th international conference, Munich, Germany, October 5-9, 2015, proceedings, part III 18,

2015, pp. 234-241: Springer.

[5] F. Milletari, N. Navab, and S.-A. Ahmadi, "V-net: Fully convolutional neural networks for volumetric medical image segmentation," in 2016 fourth international conference on 3D vision (3DV), 2016, pp. 565-571: IEEE.

[6] A. R. Benaim et al., "Analyzing medical research results based on synthetic data and their relation to real data results: systematic comparison from five observational studies," JMIR medical informatics, vol. 8, no. 2, p. e16492, 2020.

[7] C. Ngufor, H. Van Houten, B. S. Caffo, N. D. Shah, and R. G. McCoy, "Mixed effect machine learning: A framework for predicting longitudinal change in hemoglobin A1c," Journal of biomedical informatics, vol. 89, pp. 56-67, 2019.

[8] T. Laderas, N. Vasilevsky, B. Pederson, M. Haendel, S. McWeeney, and D. A. Dorr, "Teaching data science fundamentals through realistic synthetic clinical cardiovascular data," BioRxiv, p. 232611, 2017.

[9] I. Goodfellow et al., "Generative adversarial nets," Advances in neural information processing systems, vol. 27, 2014.

[10] D. Hennessy, C. Sanmartin, S. Eftekhary, L. Plager, J. Jones, and K. Onate, "Creating a synthetic database for use in microsimulation models to investigate alternative health care financing strategies in Canada," Int J. Microsimul, vol. 8, pp. 41-74, 2015.

[11] M. Giuffrè and D. L. Shung, "Harnessing the power of synthetic data in healthcare: innovation, application, and privacy," NPJ digital medicine, vol. 6, no. 1, p. 186, 2023.

[12] D. Rankin, M. Black, R. Bond, J. Wallace, M. Mulvenna, and G. Epelde, "Reliability of supervised machine learning using synthetic data in health care: Model to preserve privacy for data sharing," JMIR medical informatics, vol. 8, no. 7, p. e18910, 2020.

[13] J. Jordon et al., "Synthetic Data--what, why and how?," arXiv preprint arXiv:2205.03257, 2022.

[14] M. Prastawa, E. Bullitt, and G. Gerig, "Simulation of brain tumors in MR images for evaluation of segmentation efficacy," Medical image analysis, vol. 13, no. 2, pp. 297-311, 2009.

[15] C. Han et al., "GAN-based synthetic brain MR image generation," in 2018 IEEE 15th international symposium on biomedical imaging (ISBI 2018), 2018, pp. 734-738: IEEE.

[16] A. Radford, L. Metz, and S. Chintala, "Unsupervised representation learning with deep convolutional generative adversarial networks. arXiv 2015," arXiv preprint arXiv:1511.06434, 2015.

[17] M. Arjovsky, S. Chintala, and L. Bottou, "Wasserstein generative adversarial networks," in International conference on machine learning, 2017, pp. 214-223: PMLR.

[18] T. Salimans, I. Goodfellow, W. Zaremba, V. Cheung, A. Radford, and X. Chen, "Improved techniques for training gans," Advances in neural information processing systems, vol. 29, 2016.

[19] S. A. Güven, Use of generative adversarial networks in medical image synthesis and segmentation, PhD Thesis, İnönü University, Turkey, 2022.

[20] M. Raja and S. Vijayachitra, "A hybrid approach to segment and detect brain abnormalities from MRI scan," Expert Systems with Applications, vol. 216, p. 119435, 2023.

[21] K. Kazuhiro et al., "Generative adversarial networks for the creation of realistic artificial brain magnetic resonance images," Tomography, vol. 4, no. 4, p. 159, 2018.

[22] E. Güvenç, G. Çetin, and M. Ersoy, "Generating Synthetic Images from Real MR Images Using Deep Learning Methods," Gazi Journal of Engineering Sciences, vol. 9, no. 4, pp. 230-239, 2023.

[23] H. H. N. Alrashedy, A. F. Almansour, D. M. Ibrahim, and M. A. A. Hammoudeh, "BrainGAN: brain MRI image generation and classification framework using GAN architectures and CNN models," Sensors, vol. 22, no. 11, p. 4297, 2022.

[24] R. Mehrotra, M. Ansari, R. Agrawal, and R. Anand, "A transfer learning approach for AI-based classification of brain tumors," Machine Learning with Applications, vol. 2, p. 100003, 2020.

[25] Y. Jiang, H. Chen, M. Loew, and H. Ko, "COVID-19 CT image synthesis with a conditional generative adversarial network," IEEE Journal of Biomedical and Health Informatics, vol. 25, no. 2, pp. 441-452, 2020.

[26] H. P. Das et al., "Conditional synthetic data generation for robust machine learning applications with limited pandemic data," in Proceedings of the AAAI Conference on Artificial Intelligence, 2022, vol. 36, no. 11, pp. 11792-11800.

[27] B. Loong, A. M. Zaslavsky, Y. He, and D. P. Harrington, "Disclosure control using partially synthetic data for large-scale health surveys, with applications to CanCORS," Statistics in medicine, vol. 32, no. 24, pp. 4139-4161, 2013.

[28] H. M. T. Khushi, T. Masood, A. Jaffar, and S. Akram, "A Novel Approach to Classify Brain Tumor with an Effective Transfer Learning based Deep Learning Model," Brazilian Archives of Biology and Technology, vol. 67, p. e24231137, 2024.

[29] O. Bouguerra, B. Attallah, and Y. Brik, "MRI-based brain tumor ensemble classification using two stage score level fusion and CNN models," Egyptian Informatics Journal, vol. 28, p. 100565, 2024.

[30] M. Ghaffari, A. Sowmya, and R. Oliver, "Automated brain tumor segmentation using multimodal brain scans: a survey based on models submitted to the BraTS 2012–2018 challenges," IEEE reviews in biomedical engineering, vol. 13, pp. 156-168, 2019.

[31] B. H. Menze et al., "The multimodal brain tumor image segmentation benchmark (BRATS)," IEEE transactions on medical imaging, vol. 34, no. 10, pp. 1993-2024, 2014.

[32] D. Zikic, Y. Ioannou, M. Brown, and A. Criminisi, "Segmentation of brain tumor tissues with convolutional neural networks," Proceedings MICCAI-BRATS, vol. 36, no. 2014, pp. 36-39, 2014.

[33] M. Havaei et al., "Brain tumor segmentation with deep neural networks," Medical image analysis, vol. 35, pp. 18-31, 2017.

[34] S. Bakas et al., "Identifying the best machine learning algorithms for brain tumor segmentation, progression assessment, and overall survival prediction in the BRATS challenge," arXiv preprint arXiv:1811.02629, 2018.

[35] F. Isensee, P. Kickingereder, W. Wick, M. Bendszus, and K. H. Maier-Hein, "Brain tumor segmentation and radiomics survival prediction: Contribution to the brats 2017 challenge," in Brainlesion: Glioma, Multiple Sclerosis, Stroke and Traumatic Brain Injuries: Third International Workshop, BrainLes 2017, Held in Conjunction with MICCAI 2017, Quebec City, QC, Canada, September 14, 2017, Revised Selected Papers 3, 2018, pp. 287-297: Springer.

[36] K. Kamnitsas et al., "DeepMedic for brain tumor segmentation," in Brainlesion: Glioma, Multiple Sclerosis, Stroke and Traumatic Brain Injuries: Second International Workshop, BrainLes 2016, with the Challenges on BRATS, ISLES and mTOP 2016, Held in Conjunction with MICCAI 2016, Athens, Greece, October 17, 2016, Revised Selected Papers 2, 2016, pp. 138-149: Springer.

[37] X. Zhao, Y. Wu, G. Song, Z. Li, Y. Fan, and Y. Zhang, "Brain tumor segmentation using a fully convolutional neural network with conditional random fields," in Brainlesion: Glioma, Multiple Sclerosis, Stroke and Traumatic Brain Injuries: Second International Workshop, BrainLes 2016, with the Challenges on BRATS, ISLES and mTOP 2016, Held in Conjunction with MICCAI 2016,

Athens, Greece, October 17, 2016, Revised Selected Papers 2, 2016, pp. 75-87: Springer.

[38] L. Weninger, O. Rippel, S. Koppers, and D. Merhof, "Segmentation of brain tumors and patient survival prediction: Methods for the brats 2018 challenge," in Brainlesion: Glioma, Multiple Sclerosis, Stroke and Traumatic Brain Injuries: 4th International Workshop, BrainLes 2018, Held in Conjunction with MICCAI 2018, Granada, Spain, September 16, 2018, Revised Selected Papers, Part II 4, 2019, pp. 3-12: Springer.

[39] M. I. Sharif, J. P. Li, M. A. Khan, and M. A. Saleem, "Active deep neural network features selection for segmentation and recognition of brain tumors using MRI images," Pattern Recognition Letters, vol. 129, pp. 181-189, 2020.

[40] J. Nalepa, M. Marcinkiewicz, and M. Kawulok, "Data augmentation for brain-tumor segmentation: a review," Frontiers in computational neuroscience, vol. 13, p. 83, 2019.

[41] Z. Jiang, C. Ding, M. Liu, and D. Tao, "Two-stage cascaded u-net: 1st place solution to brats challenge 2019 segmentation task," in Brainlesion: Glioma, Multiple Sclerosis, Stroke and Traumatic Brain Injuries: 5th International Workshop, BrainLes 2019, Held in Conjunction with MICCAI 2019, Shenzhen, China, October 17, 2019, Revised Selected Papers, Part I 5, 2020, pp. 231-241: Springer.

[42] H.-M. Chen et al., "Comparison of Multispectral Image-Processing Methods for Brain Tissue Classification in BrainWeb Synthetic Data and Real MR Images," BioMed Research International, vol. 2021, no. 1, p. 9820145, 2021.

[43] R. Anitha and D. Siva Sundhara Raja, "Development of computer-aided approach for brain tumor detection using random forest classifier," International Journal of Imaging Systems and Technology, vol. 28, no. 1, pp. 48-53, 2018.

[44] M. Sharif, U. Tanvir, E. U. Munir, M. A. Khan, and M. Yasmin, "Brain tumor segmentation and classification by improved binomial thresholding and multi-features selection," Journal of ambient intelligence and humanized computing, pp. 1-20, 2024.

[45] S. Basheera and M. Satya Sai Ram, "Classification of brain tumors using deep features extracted using CNN," in Journal of Physics: Conference Series, 2019, vol. 1172, p. 012016: IOP Publishing.

[46] Y. K. Chandra and A. Agrawal, "Deep learning based brain tumor segmentation and classification using MRI images," in 2022 Third International Conference on Intelligent Computing Instrumentation and Control Technologies (ICICICT), 2022, pp. 1248-1254: IEEE.

[47] M. S. Fuad, C. Anam, K. Adi, and G. Dougherty, "Comparison of two convolutional neural network models for automated classification of brain cancer types," in AIP Conference Proceedings, 2021, vol. 2346, no. 1: AIP Publishing.

[48] S. Kadry, R. Damaševičius, D. Taniar, V. Rajinikanth, and I. A. Lawal, "Extraction of tumour in breast MRI using joint thresholding and segmentation–A study," in 2021 Seventh International conference on Bio Signals, Images, and Instrumentation (ICBSII), 2021, pp. 1-5: IEEE.

[49] J. Amin, M. Sharif, M. Yasmin, and S. L. Fernandes, "A distinctive approach in brain tumor detection and classification using MRI," Pattern Recognition Letters, vol. 139, pp. 118-127, 2020.

[50] A. Kujur, Z. Raza, A. A. Khan, and C. Wechtaisong, "Data complexity based evaluation of the model dependence of brain MRI images for classification of brain tumor and Alzheimer's disease," IEEE Access, vol. 10, pp. 112117-112133, 2022.

[51] J. Acquarelli et al., "Convolutional neural networks to predict brain tumor grades and Alzheimer's disease with MR spectroscopic imaging data," Plos one, vol. 17, no. 8, p. e0268881, 2022.

[52] A. Ashraf, Z. Qingjie, W. H. K. Bangyal, and M. Iqbal, "Analysis of brain imaging data for the detection of early age autism spectrum disorder using transfer learning approaches for internet of things," IEEE Transactions on Consumer Electronics, vol. 70, no. 1, pp. 4478-4489, 2023.

[53] X. Li, Y. Gu, N. Dvornek, L. H. Staib, P. Ventola, and J. S. Duncan, "Multi-site fMRI analysis using privacy-preserving federated learning and domain adaptation: ABIDE results," Medical image analysis, vol. 65, p. 101765, 2020.

[54] Z. N. K. Swati et al., "Brain tumor classification for MR images using transfer learning and fine-tuning," Computerized Medical Imaging and Graphics, vol. 75, pp. 34-46, 2019.

[55] M. M. Zahoor et al., "A new deep hybrid boosted and ensemble learning-based brain tumor analysis using MRI," Sensors, vol. 22, no. 7, p. 2726, 2022.

[56] Y. Gusev, K. Bhuvaneshwar, L. Song, J.-C. Zenklusen, H. Fine, and S. Madhavan, "The REMBRANDT study, a large collection of genomic data from brain cancer patients," Scientific data, vol. 5, no. 1, pp. 1-9, 2018.

[57] L. Shen and T. Anderson, "Multimodal brain MRI tumor segmentation via convolutional neural networks," vol, vol. 18, pp. 2014-2015, 2017.

[58] K. Özdem et al., "A ga-based cnn model for brain tumor classification," in 2022 7th International Conference on Computer Science and Engineering (UBMK), 2022, pp. 418-423: IEEE.

[59] A. G. Eker, G. K. Erdem, and N. Duru, "Categorical and Binary Brain Tumor Classification Using Transfer Learning Techniques," Sivas Cumhuriyet University Journal of the Faculty of Engineering, vol. 1, no. 1, pp. 11-16, 2023.

[60] H. E. Kim, A. Cosa-Linan, N. Santhanam, M. Jannesari, M. E. Maros, and T. Ganslandt, "Transfer learning for medical image classification: a literature review," BMC medical imaging, vol. 22, no. 1, p. 69, 2022.

[61] G. Huang, Z. Liu, L. Van Der Maaten, and K. Q. Weinberger, "Densely connected convolutional networks," in Proceedings of the IEEE conference on computer vision and pattern recognition, 2017, pp. 4700-4708.

[62] F. Chollet, "Xception: Deep learning with depthwise separable convolutions," in Proceedings of the IEEE conference on computer vision and pattern recognition, 2017, pp. 1251-1258.

[63] K. Simonyan and A. Zisserman, "Very deep convolutional networks for large-scale image recognition," arXiv preprint arXiv:1409.1556, 2014.

[64] F. Doğan and İ. Türkoğlu, "Derin öğrenme modelleri ve uygulama alanlarına ilişkin bir derleme," Dicle Üniversitesi Mühendislik Fakültesi Mühendislik Dergisi, vol. 10, no. 2, pp. 409-445, 2019.

[65] T. S. Azzahra, J. J. Cerelia, F. A. L. Nugraha, and A. A. Pravitasari, "MRI-based brain tumor classification using inception resnet V2," Enthusiastic: International Journal of Applied Statistics and Data Science, pp. 163-175, 2023.

[66] S. Mascarenhas and M. Agarwal, "A comparison between VGG16, VGG19 and ResNet50 architecture frameworks for Image Classification," in 2021 International conference on disruptive technologies for multi-disciplinary research and applications (CENTCON), 2021, vol. 1, pp. 96-99: IEEE.

[67] A. Younis et al., "Abnormal brain tumors classification using resnet50 and its comprehensive evaluation," IEEE Access, vol. 12, pp. 78843-78853, 2024.

[68] R. Pillai, A. Sharma, N. Sharma, and R. Gupta, "Brain tumor classification using VGG 16, ResNet50, and inception V3 transfer learning models," in 2023 2nd International Conference for Innovation in Technology (INOCON), 2023, pp. 1-5: IEEE.

[69] D. S. Wankhede, C. J. Shelke, V. K. Shrivastava, R. Achary, and S. N. Mohanty, "Brain Tumor Detection and Classification Using Adjusted InceptionV3, AlexNet, VGG16, VGG19 with ResNet50-152 CNN Model," EAI Endorsed Transactions on Pervasive Health & Technology, vol. 10, no. 1, 2024.

[70] M. T. R. Shawon, G. S. Shibli, F. Ahmed, and S. K. S. Joy, "Explainable cost-sensitive deep neural networks for brain tumor detection from brain mri images considering data imbalance," Multimedia Tools and Applications, pp. 1-28, 2025.

[71] M. Celik and O. Inik, "Development of hybrid models based on deep learning and optimized machine learning algorithms for brain tumor Multi-Classification," Expert Systems with Applications, vol. 238, p. 122159, 2024.

[72] S. Moldovanu, G. Tăbăcaru, and M. Barbu, "Convolutional neural Network–Machine learning model: hybrid model for meningioma tumour and healthy brain classification," Journal of Imaging, vol. 10, no. 9, p. 235, 2024.

[73] A. F. Al Bataineh et al., "Enhanced magnetic resonance imaging-based brain tumor classification with a hybrid Swin Transformer and ResNet50V2 model," Applied Sciences, vol. 14, no. 22, p. 10154, 2024.

[74] K. Mahmut, Bilgisayar Bilimlerinde Güncel Konular ve Yeni Nesil Teknolojiler. Akademisyen Kitabevi, 2022.

[75] A. Dash, J. Ye, and G. Wang, "A review of generative adversarial networks (GANs) and its applications in a wide variety of disciplines: from medical to remote sensing," IEEE Access, 2023.

[76] G. Degottex and M. Gales, "A Spectrally Weighted Mixture of Least Square Error and Wasserstein Discriminator Loss for Generative SPSS," in 2018 IEEE Spoken Language Technology Workshop (SLT), 2018, pp. 603-609: IEEE.

[77] Y. Canbay, S. Adsiz, and P. Canbay, “Privacy-preserving transfer learning framework for kidney disease detection,” Applied Sciences, vol. 14, no. 19, Art. no. 8629, 2024.